BULETINUL INSTITUTULUI POLITEHNIC DIN IAŞI
Publicat de
Universitatea Tehnică „Gheorghe Asachi” din Iaşi
Volumul 69 (73), Numărul 1, 2023
Secţia
CONSTRUCŢII DE MAŞINI
DOI:10.2478/bipcm-2023-0002

A STUDY ON TOOL PATH GENERATION IN 2D CONTOUR MILLING OF CYCLOIDAL DISCS AND RINGS USED IN CYCLOIDAL REDUCERS

BY

MIHĂIȚĂ HORODINCĂ*

“Gheorghe Asachi” Technical University of Iași,
Faculty of Machine Manufacturing and Industrial Management, Digital Manufacturing Systems Department, D. Mangeron 59A, 700050, Iași, Romania

Received: February 3, 2023
Accepted for publication: March 4, 2023

Abstract. This paper presents a study on the determination of the tool paths in manufacturing by external or internal 2D contour milling (using an end mill cutter as tool) of a cycloidal disc and a cycloidal ring used inside a cycloidal reducer in two versions: with rotary pins as gear teeth placed on stator (in gear with cycloidal disc) and with rotary pins placed on rotor (in gear with cycloidal ring). These tool paths should be described by the Cartesian coordinates of the points on the 2D closed trajectory of the tool axis. The 2D profiles of a cycloidal disc (or a cycloidal ring) in transverse section and an analytic geometric approach are used in order to find out these tool paths, having a shape of distorted epicycloids or hypocycloids. Even though this goal is simply solvable on CNC milling machines by cutting radius compensation, some particularities of 2D profiles for a cycloidal disc (or a cycloidal ring) impose a specific theoretical approach on this topic. Some algorithms for tool path detection were proposed, verified and validated by simulation in Matlab on both 2D profiles.

---

*Corresponding author; *e-mail*: horodinca@tuiasi.ro

Keywords: Cycloidal reducer, cycloidal disc, cycloidal ring, 2D profile, 2D contour milling, tool path.

1. Introduction

A well-known particularity of a cycloidal reducer is the using of Z_S rotary cylindrical pins (or pinwheels) as gear teeth placed on a gear ring (Allotta *et al*., 2021; Dion *et al*., 2020; Lai, 2022). This involves an appropriate outer shape of the rotor (or cycloidal disc as well) with $Z_R= Z_S$-1 lobes, working as gear against the ring. Each rotor lobe plays the role of a gear tooth. This outer shape is parametrically describable as a 2D profile in transverse section by Shin J.H. and Kwon S.M (2006) and Petrovic N. *et al.* (2013). This parametric description allows the profile optimization for different purposes, e.g.: pressure angle distribution characteristics (Li *et al*., 2020), backlash optimization (Lu *et al*., 2018), minimizing the volume and maximize the power efficiency (Wang *et al*., 2016), etc. A study on the description of the cycloidal disc 2D profile in transverse section (a distorted epicycloid) revealed by computer aided geometrical simulation was done in a previous work (Horodinca *et al*., 2022a), mainly for manufacturing purposes.

The coordinates of the points placed on the cycloidal disc 2D profile are useful in manufacturing on CNC machines by external 2D contour milling using an end mill cutter as tool. The coordinates of points involved in the description of milling tool axis trajectory (or tool path as well, as an outer offset of the 2D profile) strictly depends by this 2D profile and the radius of end mill tool. These coordinates are usually calculated by so called cutting radius (tool size) compensation methods, a topic well covered by literature (Yue and Yu, 2011; Han *et al*., 2013), inclusively with CAD and CAM software facilities and frequently on CNC machines (with G41, and G42 commands in G-code, https://cnc-programming-tips.blogspot.com/2014/12/g40-g41-and-g42-cuttercompensation.html). Despite these opportunities, we found that a particular study on the tooth path geometry in cycloidal disc manufacturing by 2D contour milling is useful, for a better understanding of cycloidal disc 2D profile geometry and eventually for design improvement. The description of tool path is obtained using some approaches based on analytic geometry applied in Matlab.

The results of this study are applicable also in tooth path detection for manufacturing by internal 2D contour milling of a cycloidal ring from a CR having rotary pins placed as gear teeth on the rotor. A method of description of the coordinates of the points on the inner 2D profile of a cycloidal ring (a distorted hypocycloid) was already proposed before in a previous work, (Horodinca *et al*., 2022b). The results of this study are also available in manufacturing by 2D contour milling of some other internal gears (e.g. sine gears, Horodinca, 2020).

Section 2 of this paper focuses on a theoretical approach on the tool path description based on analytic geometry. Section 3 presents some results and discussions on Matlab simulations of the tool paths used in external gear surface manufacturing on a cycloidal disc. Section 4 presents some results and discussions on Matlab simulations of the tool paths used in internal gear surface manufacturing for a cycloidal ring. Section 5 presents the conclusions and the future work.

2. Some Theoretical Approaches on the Tool Path Definition

There is a very simple approach on the tool path used for a cycloidal disc manufacture on gear surface having a known 2D profile: this path should be defined as a closed curve having an offset to the exterior against the 2D profile equal with the radius of the end mill cutter. Similarly, the tool path used for a cycloidal ring manufacture on gear surface having a known 2D profile should be defined as a closed curve having an offset to the interior against this profile equal with the radius of the end mill cutter. A first scenario related by the tool path geometry is presented in Fig. 1.

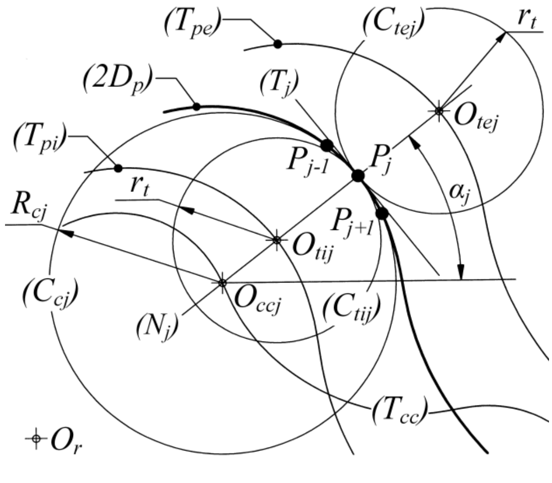

Fig. 1 – A first scenario related by tool path definition n in 2D contour milling.

Let P_{j-1}, P_j and P_{j+1} be three successive generic points placed on a 2D profile (which should be materialized on cycloidal disc or on cycloidal ring, as ($2D_p$) curve on Fig. 1) with known coordinates in a fixed Cartesian coordinate system (as FCCS). Let is (C_{cj}) the circle defined by these three generic points, with the center in O_{ccj}. The radius R_{cj} of this circle is exactly the radius of curvature of 2D profile in the point P_j. The normal (N_j) to the 2D profile is a straight line defined by the points O_{ccj} and P_j. The tangent line (T_j) to the 2D profile in P_j is obviously perpendicular on the normal line (N_j).

The internal 2D contour milling (e.g. for a cycloidal ring manufacture, with a reference point O_r placed permanently outside the ring, e.g. as a center of ($2D_p$)) using an end mill cutter as tool (with radius r_t) supposes to have the 2D transverse section of tool (here the circle (C_{tij})) tangent in P_j to ($2D_p$) and to (T_j) as well. This means that the center O_{tij} of the circle (C_{tij}) should be mandatory placed on the normal (N_j) as against the point O_{ccj} at a distance $d_{O_{ccj}-O_{tij}} = R_{cj} - r_t$. Each three successive points P_{j-1}, P_j and P_{j+1} on ($2D_p$) profile describe a point O_{tij} of the tool path (T_{pi}) during the internal 2D contour milling. The previously defined point O_{ccj} is placed on a (T_{cc}) trajectory. The radius R_{cj} and the trajectory (T_{cc}) describe the local curvature evolution of the ($2D_p$) profile.

The external 2D contour milling (e.g. for cycloidal disc manufacture, with a reference point O_r placed permanently inside the disc, e.g. as a center of ($2D_p$)) using an end mill cutter as tool (with radius r_t) supposes to have the 2D transverse section of tool (the circle (C_{tej})) tangent in P_j to ($2D_p$) and to (T_j) as well. This means that the center O_{tej} of the circle (C_{tej}) should be mandatory placed on the normal (N_j) as against the point O_{ccj} at a distance $d_{O_{ccj}-O_{tij}} = R_{cj} + r_t$. Each three successive points P_{j-1}, P_j and P_{j+1} on ($2D_p$) describe a point O_{tej} of the tool path (T_{pe}) during the external 2D contour milling.

A second scenario related by the tooth path geometry is presented in Fig. 2. Similarly with Fig. 1, here the same notations of the geometrical elements (curves, lines and points) were used.

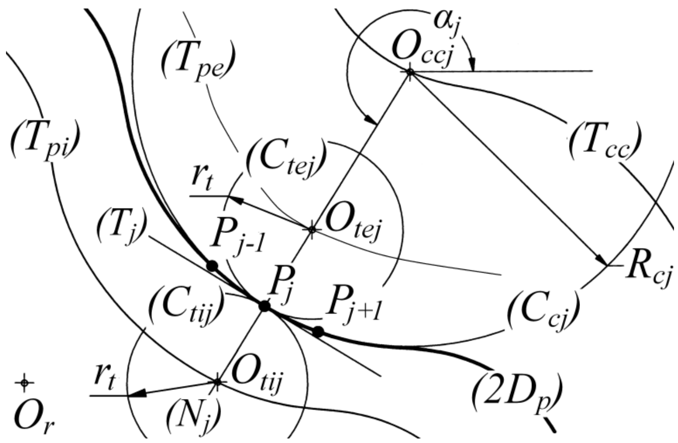

Fig. 2 – A second scenario related by tool path definition in 2D contour milling.

In this second scenario all the above considerations remain valid except the final conclusions. The center O_{tij} of the circle (C_{tij}) should be mandatory placed on the normal (N_j) as against the point O_{ccj} but in contradiction with Fig. 1, for internal milling, at a distance $d_{O_{ccj}-O_{tij}} = R_{cj}+r_t$ and for external milling at a distance $d_{O_{ccj}-O_{tij}} = R_{cj}-r_t$. Surely this contradiction (or indetermination as well) must be solved somehow.

There is a first simple available approach to solve this contradiction for internal 2D contour milling apparently in four different factual situations:

Im1. If the distance between the points O_r and P_j (as $d_{O_r-P_j}$) is bigger than the distance between the points O_r and O_{ccj} (as $d_{O_r-O_{ccj}}$), according with the first scenario, from Fig. 1, than $d_{O_{ccj}-O_{tij}} = R_{cj} - r_t$. In a simpler form, for internal milling, if $d_{O_r-P_j} > d_{O_r-O_{ccj}}$ then $d_{O_{ccj}-O_{tij}} = R_{cj} - r_t$, with O_{tij} placed on (N_j) between P_j and O_{ccj}.

Im2. If the distance between the points O_r and P_j (as $d_{O_r-P_j}$) is smaller than the distance between the points O_r and O_{ccj} (as $d_{O_r-O_{ccj}}$), according with the second scenario from Fig. 2, than $d_{O_{ccj}-O_{tij}} = R_{cj} + r_t$. In a simpler form, for internal milling, if $d_{O_r-P_j} < d_{O_r-O_{ccj}}$ then $d_{O_{ccj}-O_{tij}} = R_{cj} + r_t$, with P_j placed on (N_j) between O_{tij} and O_{ccj}.

Similarly, there is a first simple available approach to solve this contradiction for external 2D contour milling:

Em1. If the distance between the points O_r and P_j (as $d_{O_r-P_j}$) is bigger than the distance between the points O_r and O_{ccj} (as $d_{O_r-O_{ccj}}$), according with the first scenario from Fig. 1, than $d_{O_{ccj}-O_{tej}} = R_{cj} + r_t$. In a simpler form, for external milling if $d_{O_r-P_j} > d_{O_r-O_{ccj}}$ then $d_{O_{ccj}-O_{tej}} = R_{cj} + r_t$, with P_j placed on (N_j) between O_{tej} and O_{ccj}.

Em2. If the distance between the points O_r and P_j (as $d_{O_r-P_j}$) is smaller than the distance between the points O_r and O_{ccj} (as $d_{O_r-O_{ccj}}$), according with the first scenario from Fig. 2, than $d_{O_{ccj}-O_{tej}} = R_{cj} - r_t$. In a simpler form, for external milling if $d_{O_r-P_j} < d_{O_r-O_{ccj}}$ then $d_{O_{ccj}-O_{tej}} = R_{cj} - r_t$, with O_{tej} placed on (N_j) between P_j and O_{ccj}.

It is assumed that the points P_{j-1}, P_j and P_{j+1} are not placed on a straight line (R_{cj} being infinite). Fortunately some simulations prove that this never happens on the ($2D_p$) curves involved in the definition of 2D profiles for cycloidal discs or rings.

The common sense places the reference point O_r in the center of the distorted epicycloid or hypocycloid ($2D_p$).

It is interesting to remark that the factual situations **Im1** and **Im2** can be rephrased together in a single one as follows:

Im12. The internal 2D contour milling of ($2D_p$) is done if $d_{O_r-P_j} > d_{O_r-O_{ccj}}$ and $d_{O_{ccj}-O_{tij}}$ is calculated as $d_{O_{ccj}-O_{tij}} = R_{cj} - r_t$, with O_{tij} placed on (N)

between P_j and O_{ccj}, or if $d_{O_r-P_j} < d_{O_r-O_{ccj}}$ and $d_{O_{ccj}-O_{tij}}$ is calculated as $d_{O_{ccj}-O_{tij}} = R_{cj} + r_t$, with P_j placed on *(N)* between O_{tij} and O_{ccj}.

Also the factual situations **Em1** and **Em2** can be rephrased together in a single one as follows:

Em12 The external 2D contour milling of ($2D_p$) is done if $d_{O_r-P_j} > d_{O_r-O_{ccj}}$ and $d_{O_{ccj}-O_{tej}}$ is calculated as $d_{O_{ccj}-O_{tej}} = R_{cj} + r_t$, with P_j placed on (N) between O_{tej} and O_{ccj}, or if $d_{O_r-P_j} < d_{O_r-O_{ccj}}$ and $d_{O_{ccj}-O_{tej}}$ is calculated as $d_{O_{ccj}-O_{tej}} = R_{cj} - r_t$, with O_{tej} placed on (N) between P_j and O_{ccj}.

Some calculation steps should gradually be browsed in order to solve **Im12** or **Em12** factual situations as follows:

CS1. The origin of FCCS is fixed in the origin of the ($2D_p$) trajectory, a distorted epicycloid (for a cycloidal disc) or a distorted hypocycloid (for a cycloidal ring) previously determined in (Horodinca *et al.*, 2022a, b). The reference point O_r is placed in this origin.

CS2. The value of curvature radius R_{cj} and the coordinates x_{ccj}, y_{ccj} of the center O_{ccj} should be calculated for all the points P_j from closed curve ($2D_p$) having the coordinates x_j and y_j. These issues are solvable taking in account the mathematical description of a circle defined with three generic successive points P_{j-1}, P_j and P_{j+1} from ($2D_p$). The formulas from http://www.ambrnet.com/TrigoCalc/Circle3D.htm are useful for these purposes.

CS3. The values α_j of angular positions of the normal lines (N_j) as against the *x-axis* should be calculated. The four quadrant inverse tangent function from Matlab (`atan2`) is used. First argument of this function should be the difference $y_j - y_{ccj}$, second argument should be the difference $x_j - x_{ccj}$.

CS4. According with **Im12**, for 2D internal milling, the coordinates x_{tij}, y_{tij} of a point O_{tij} placed on the path (T_{pi}) are calculated as:
- $x_{tij} = x_j - r_t \cdot \cos(\alpha_j)$ and $y_{tij} = y_j - r_t \cdot \sin(\alpha_j)$ if $d_{O_r-P_j} > d_{O_r-O_{ccj}}$
- or as $x_{tij} = x_j + r_t \cdot \cos(\alpha_j)$ and $y_{tij} = y_j + r_t \cdot \sin(\alpha_j)$ if $d_{O_r-P_j} < d_{O_r-O_{ccj}}$.

CS5. According with **Em12**, for 2D external milling, the coordinates x_{tej}, y_{tej} of a point O_{tej} placed on the path (T_{pe}) are calculated as:
- $x_{tej} = x_j + r_t \cdot \cos(\alpha_j)$ and $y_{tej} = y_j + r_t \cdot \sin(\alpha_j)$ if $d_{O_r-P_j} > d_{O_r-O_{ccj}}$
- or as $x_{tej} = x_j - r_t \cdot \cos(\alpha_j)$ and $y_{tej} = y_j - r_t \cdot \sin(\alpha_j)$ if $d_{O_r-P_j} < d_{O_r-O_{ccj}}$.

It is important to note that there is a well-known mandatory required condition to accomplish in every internal and external 2D contour milling (particularly for cycloidal discs and rings): r_t<r_{min}. For both 2D contour milling (external milling in manufacturing of a cycloidal disc and internal milling in manufacturing of a cycloidal ring) $r_{min}=r_p$ with r_p being the radius of rotary pins. This will be proved in Sections 3 and 4.

These previous defined calculation steps (**CS1** ÷ **CS5**) were included in two algorithms: **AIm12** used for tool path detection in 2D contour internal milling of a cycloidal ring and **AEm12** used for tool path detection in 2D contour external milling of a cycloidal disc. These algorithms were used in Matlab program for simulation.

It is interesting that there is a simpler solution to solve **Im12** and **Em12** factual situations. The calculation steps **CS1** ÷ **CS3** previously defined are maintained (and renamed **CS1a** ÷ **CS3a**). Some supplementary steps are added:

CS4a. As it is clearly indicated in Fig. 1 and Fig. 2, for each generic point P_j two different circles ((C_{tij}) and (C_{tej})) can be generated. Let us rename these circles (C_{1j}) and (C_{2j}), their centers O_{1j} and O_{2j}, their radii R_{1j} and R_{2j} and the coordinates of their centers x_{1j}, y_{1j} and x_{2j}, y_{2j}. The calculation of these coordinates is done in a manner already described before in right side equations from **CS4** and **CS5** as: $x_{1j}=x_j-r_t\cdot\cos(\alpha_j)$, $y_{1j}=y_j-r_t\cdot\sin(\alpha_j)$ for circle (C_{1j}) and $x_{2j}=x_j+r_t\cdot\cos(\alpha_j)$, $y_{2j}=y_j+r_t\cdot\sin(\alpha_j)$ for circle (C_{2j}). The distance between the point O_{1j} and the origin of FCCS is calculated as $d_{1j} = \sqrt{x_{1j}^2 + y_{1j}^2}$. The distance between the point O_{2j} and the origin of FCCS is calculated as $d_{2j} = \sqrt{x_{2j}^2 + y_{2j}^2}$.

CS5a. For internal milling (as **Im**) the generic point O_{tij} of the tool path (T_{pi}) has the coordinates x_{tij}, y_{tij} defined as:

- if $d_{1j} < d_{2j}$ then $x_{tij}=x_{1j}=x_j-r_t\cdot\cos(\alpha_j)$ and $y_{tij}=y_{1j}=y_j-r_t\cdot\cos(\alpha_j)$;
- if $d_{2j} < d_{1j}$ then $x_{tij}=x_{2j}=x_j+r_t\cdot\cos(\alpha_j)$ and $y_{tij}=y_{2j}=y_j+r_t\cdot\cos(\alpha_j)$;

CS6a. For external milling (as **Em**) the generic point O_{tej} of the tool path (T_{pe}) has the coordinates x_{tej}, y_{tej} defined as:

- if $d_{1j} > d_{2j}$ then $x_{tej}=x_{1j}=x_j-r_t\cdot\cos(\alpha_j)$ and $y_{tej}=y_{1j}=y_j-r_t\cdot\cos(\alpha_j)$;
- if $d_{2j} > d_{1j}$ then $x_{tej}=x_{2j}=x_j+r_t\cdot\cos(\alpha_j)$ and $y_{tej}=y_{2j}=y_j+r_t\cdot\cos(\alpha_j)$;

These **CS1a** ÷ **CS6a** calculation steps were also included in two algorithms: **AIm** used for tool path detection in 2D contour internal milling of a cycloidal ring and **AEm** used for tool path detection in 2D contour external milling of a cycloidal disc.

These last defined algorithms (**AIm** and **AEm**) were used also for simulation using some computer program for Matlab. Some results in simulation are presented in next paper sections (3 and 4).

3. Some Results and Discussions on Simulations of the Tool Path Used in Manufacturing of a Cycloidal Disc (by External 2D Contour Milling)

A zoomed-in detail on a Matlab simulation for (T_{pe}) detection by **AEm12** algorithm useful for external 2D contour milling manufacture of the gear surface on a cycloidal disc is presented in Fig. 3. The ($2D_p$) profile (described with 10,000 points P_j) was provided by a previously study (Horodinca *et al.*, 2022a), for a cycloidal disc with Z_R=14 lobes as gear teeth in gear with a stator with Z_S=15 equidistant rotary pins (with r_p=5 mm radius) placed on a circle with r_{pp}= 47.8339 mm radius, calculated as $r_{pp}=r_p/[\sin(\pi/2 \cdot Z_S)]$. The ($2D_p$) profile is slightly smoothed using a moving average filter (five values in the average) for abscissae and ordinates of points placed on ($2D_p$). There is no profile shift for stator (s=0), a milling tool with radius r_t=4 mm was used.

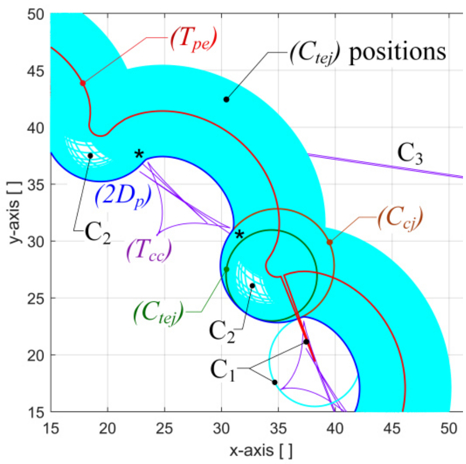

Fig. 3 – A zoomed-in detail on (T_{pe}) detection for a cycloidal disc (s=0) using **AEm12** algorithm.

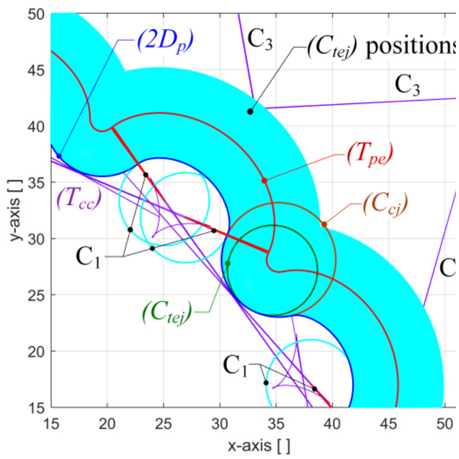

Fig. 4 – A zoomed-in detail on (T_{pe}) detection for a cycloidal disc with positive shifting (s=5 mm) using **AEm12** algorithm.

The notations from Fig. 1 and Fig. 2 (except C_1, C_2 and C_3) are used here. Figure 4 presents the same simulation but with a positive shift of s=5 mm for stator profile.

The main reason of this profile shifting from Fig. 4 is the disappearance of the discontinuity points (marked with * on Fig. 3) for the benefit of cycloidal reducer optimal operation. The cyan coloured region indicates in both Figures all the positions (9.999 positions) of the circles (C_{tej}). The main considerations done before in **AEm12** algorithm are confirmed here, except those indicated by labels C_1. As expected the edging to the inside of this region is the $(2D_p)$.

Some important irregularities related by (T_{pe}) path shape are flagged with the labels C_1 in both Figures. With certainty they indicate errors in the determination of (T_{pe}) path. This means that **Em2** and by consequence **AEm12** doesn't produces correct situations for some particularly positions of the generic points $P_{j\text{-}1}$, P_j and P_{j+1}, in other words the conclusion form **Em2** if $d_{O_r-P_j} < d_{O_r-O_{ccj}}$ then $d_{O_{ccj}-O_{tej}} = R_{cj} - r_t$, is contradicted in some points on (T_{pe}) path. It is not relevant to find out an explanation for these errors because as we will see later the **Em**, and **AEm** eliminates these irregularities, as Fig. 5 and Fig. 6 clearly indicate. Probably in that points should be used **Im2** and **AEm12**.

The regions depicted by C_2 in Fig. 3 indicates that the circles (C_{tej}) are not uniform distributed over the (T_{pe}) path, in other words the speed of milling tool axis (feed rate) on (T_{pe}) path is higher as usual in that region. This C_2 shortcoming of (T_{pe}) path is strongly reduced in Fig. 4. The regions depicted with C_3 in both Figures indicate that there are some local anomalies on (T_{cc}) trajectory due to the fact that the $(2D_p)$ is not described as a smooth profile; it has a certain roughness, strongly amplified on (T_{cc}). If the CNC milling machine is able to exactly reproduced the (T_{pe}) path then the manufactured $(2D_p)$ and the theoretical one should have similar roughness.

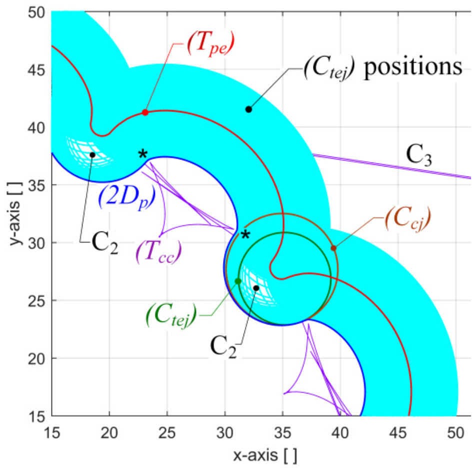

Fig. 5 – A zoomed-in detail on (T_{pe}) detection for a cycloidal disc ($s=0$) using the **AEm** algorithm.

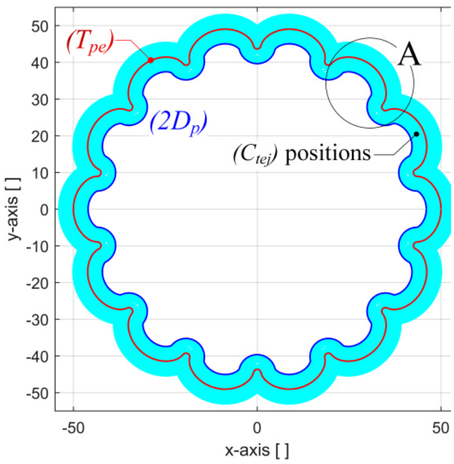

Fig. 6 – The $(2D_p)$, (T_{pe}) paths and (C_{tej}) positions for the entire cycloidal disc from Fig. 5.

Figure 5 presents a similar simulation as previously was done in Fig. 3, but this time using the **AEm** algorithm. It is obvious that the C_1 irregularity completely disappears here. This is more evident in Fig. 6 which presents the entire $(2D_p)$ profile of cycloidal disc, the (T_{pe}) path and all (C_{tej}) positions.

Figure 5 is a zoomed-in detail of Fig. 6 from the area labelled with A.

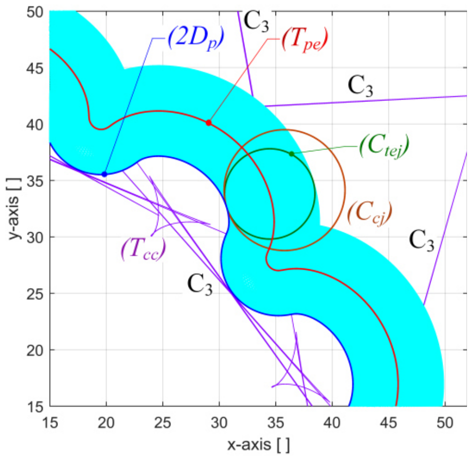

Fig. 7 – A zoomed-in detail on (T_{pe}) detection for a cycloidal disc (s=5 mm) using the **AEm** algorithm.

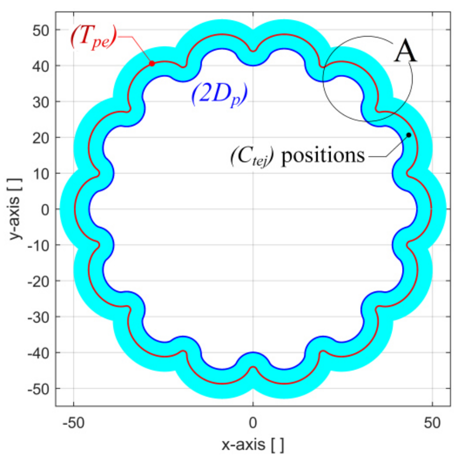

Fig. 8– The ($2D_p$), (T_{pe}) paths and (C_{tej}) positions for the entire cycloidal disc from Fig. 7.

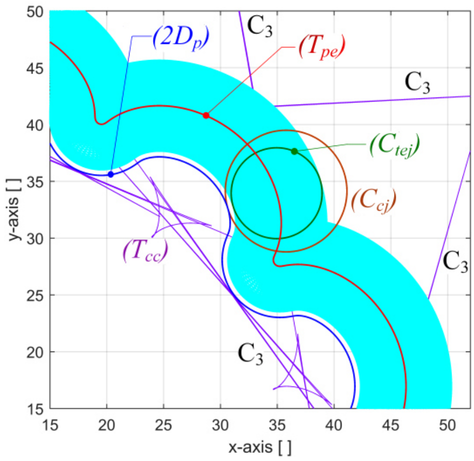

Fig. 9 – A zoomed-in detail on (T_{pe}) detection for a cycloidal disc manufacture (s=5 mm and milling allowance a=0.5 mm) using the **AEm** algorithm.

It is clear that **AEm** algorithm produces perfect results, better than **AEm12**. This conclusion is confirmed in Fig. 7 and Fig. 8. These Figures are similar to Fig. 5 and Fig. 6 respectively but for s=5 mm as shift profile. Figure 7 is a zoomed-in detail of Fig. 8 from the area labelled with A.

It is obvious that the external active surface of the cycloidal disc (working as gear) should be manufactured with several successive machining sequences by 2D contour milling; a milling allowance is left (this active surface is intentionally oversized) between each two sequences.

There is a simple way to detect the (T_{pe}) path in this approach. For example, in external 2D contour milling the (T_{pe}) path with an allowance a before a final milling sequence is defined with a conceptual milling tool having the radius r_t+a but the manufacturing is done with a real tool having the radius r_t. Figure 9 describes with a zoom-in detail (similarly with Fig. 5 and Fig. 7) this approach (with a=0.5 mm). It is obvious that the internal envelope of the positions of circles (C_{cj}) is shifted outside ($2D_p$) profile with a distance a.

The consequences of violation of the constrain $r_t<r_p$ for external milling can be highlighted by simulation. Figure 10 presents the (T_{pe}) path, the ($2D_p$) trajectory and all positions (C_{tej}) for cycloidal disc manufacturing (in conditions used before in Fig. 7 for simulation) with $r_t=r_p$. There are no negative consequences on ($2D_p$) profile. However this situation $r_t=r_p$ is to be avoided in practice (especially for small values of s) because with high probability may appears dynamic instability of milling process (chatter) when the milling tool is placed in concave regions of ($2D_p$) profile, where the circles (C_{tej}) and (C_{cj}) having almost similar radius.

Figure 11 presents the (T_{pe}) path, the ($2D_p$) trajectory and all positions (C_{tej}) for cycloidal disc manufacturing (in conditions used before in Fig. 7 for simulation) also with the violation of the condition now with $r_t>r_p$ (with r_t=5.5 mm as against r_p=5 mm).

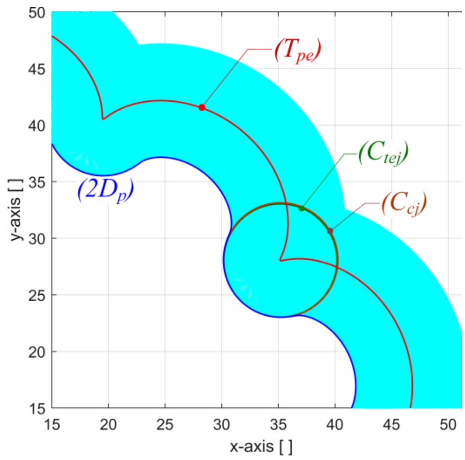

Fig. 10 – A zoomed-in detail on (T_{pe}) detection for the cycloidal disc (s=5 *mm* and $r_t=r_p$=5 mm) using the **AEm** algorithm.

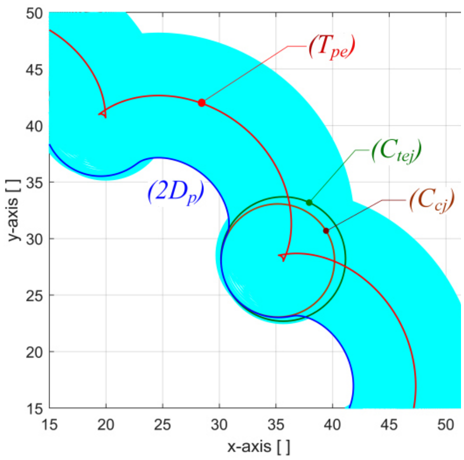

Fig. 11 – A zoomed-in detail on (T_{pe}) detection for the cycloidal disc (s=5 mm and $r_t>r_p$ with r_t=5.5 mm) using the **AEm** algorithm.

It is evident that this time the ($2D_p$) profile definition by milling is wrong, the internal envelope of all (C_{tej}) positions (with the centers placed on (T_{pe}) path, having here a particularly shape) is different (shifted inside in some regions) as against the correct ($2D_p$) trajectory. In concave regions of the ($2D_p$) profile there is an undesired interference with the milling tool.

It is interesting to note the evolution of (T_{pe}) path shape as distorted epicycloid in different situations exposed in this section.

4. Some Results and Discussions on Simulations of the Tool Paths Used in Manufacturing of a Cycloidal Ring (by Internal 2D Contour Milling)

A zoomed-in detail on a Matlab simulation for (T_{pe}) detection by **AIm12** algorithm useful for internal 2D contour milling manufacture of the gear surface on a cycloidal ring is presented in Fig. 12. The ($2D_p$) profile (described with 10,000 points P_j) was provided by a previously study (Horodinca *et al.*, 2022b), for a cycloidal ring with Z_S=15 lobes as gear teeth in gear with a rotor with Z_R=14 equidistant rotary pins (r_p=5 mm radius) as gear teeth on rotor, placed on a circle with r_{pp}= 47.8339 mm radius, calculated as $r_{pp}=r_p/[\sin(\pi/2\cdot Z_R)]$. The ($2D_p$) profile was slightly smoothed using a moving average filter (five values in the average) for abscissae and ordinates of points placed on ($2D_p$). There is no profile shift for rotor (s=0), a milling tool with r_t=4 mm radius was used.

Figure 13 presents the same simulation based on **AIm12** but with a positive shift of s=5 mm for rotor profile.

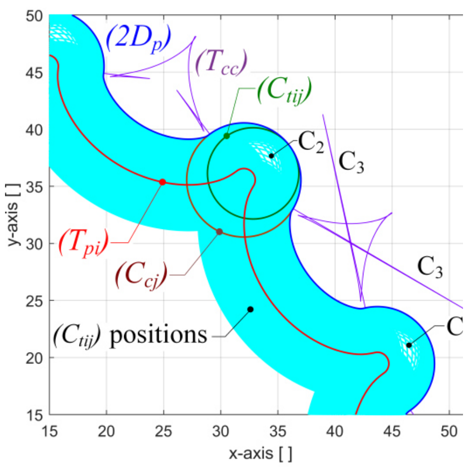

Fig. 12 – A zoomed-in detail on (T_{pi}) detection for a cycloidal ring (s=0) using the **AIm12** algorithm.

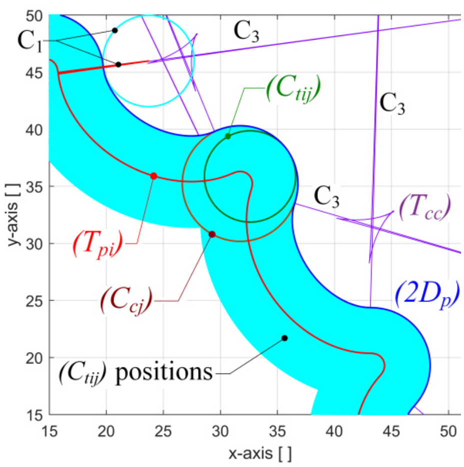

Fig. 13 – A zoomed-in detail on (T_{pi}) detection for a cycloidal ring (s=5mm) using the**AIm12** algorithm.

By comparison with Fig. 3, the (T_{pi}) path from Fig. 12 is appropriately determined. The discontinuity C_1 on (T_{pe}) path revealed on Fig. 3 doesn't exists here on (T_{pi}) path. The external envelope of all family of (C_{tij}) circles is exactly ($2D_p$). However this discontinuity C_1 (as error on (T_{pi}) path) occurs if a positive shift of rotor profile is used as Fig. 13 proves. This means that similarly with **AEm12**, the **AIm12** algorithm is not perfect.

Figure 14 show that these discontinuities C_1 occurs systematically on the entire (T_{pi}) path. Figure 13 is a zoomed-in detail of Fig. 14 from area labelled with A.

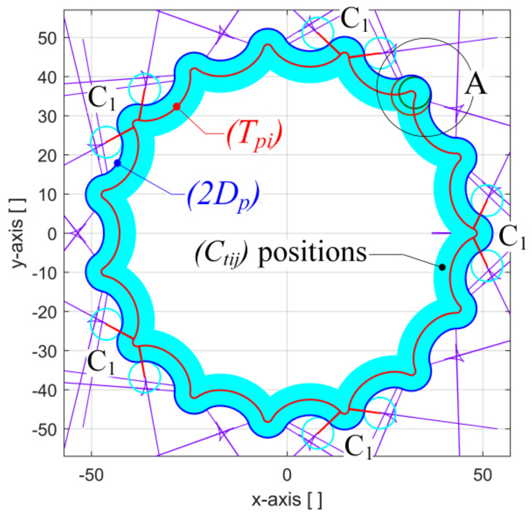

Fig. 14 – The ($2D_p$), (T_{pi}), (T_{cc}) paths and (C_{tij}) positions for the entire cycloidal ring from Fig. 13.

Similarly with the solution found in section 3 of this paper in order to eliminate the C_1 errors (**AEm12** replaced by **AEm** algorithm) the using of **AIm** algorithm (instead **Aim12**) is an appropriate option here.

This is proved by simulation results from Fig. 15, and Fig. 16. Figure 15 is an equivalent of Fig. 13, Fig. 16 is an equivalent of Fig. 14, both Figures using the **AIm** algorithm.

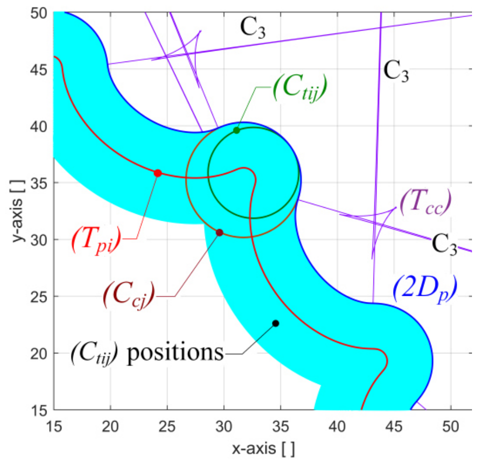

Fig. 15 – A zoomed-in detail on (T_{pi}) detection for a cycloidal ring (s=5 mm) using the **AIm** algorithm. For comparison with Fig. 13.

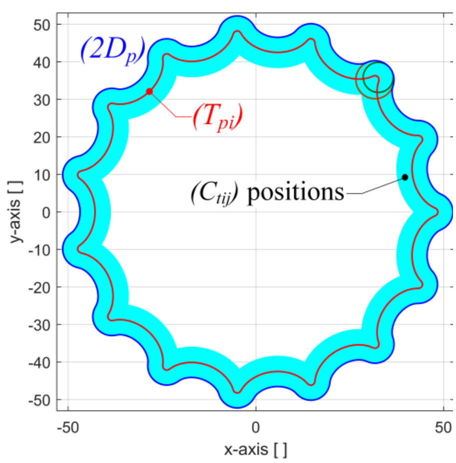

Fig. 16 – The ($2D_p$), (T_{pi}) paths and (C_{tij}) positions for the entire cycloidal ring from Fig. 15. For comparison with Fig. 14.

As can be seen quite clearly on both Figures, now the discontinuities C_1 completely disappear.

Similarly with the study performed in section 3, the effects of violation for the mandatory condition $r_t<r_p$ in internal milling can be highlighted by

simulation. In Fig. 17 the result of $r_t=r_p$ simulation (here r_p=5 mm) is revealed. Even the (T_{pi}) path is correctly generated as is clearly indicated, in convex regions (from the point of view of an outside observer, or in concave regions from the point of view of an inside observer) where the circles (C_{tej}) and (C_{cj}) have almost similar radius (especially for small values of s), there is a high risk of dynamic instability during 2D contour milling (known in cutting processes as chatter).

In Fig. 18 the result of the violation of mandatory condition $r_t<r_p$ by simulation (with $r_t>r_p$ r_t=5.5 mm and r_p=5 mm) was revealed. It is clear here that a wrong definition of ($2D_p$) profile was obtained in some regions.

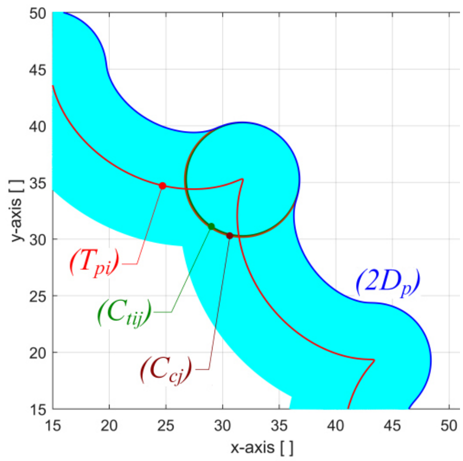

Fig. 17 – A zoomed-in detail on (T_{pi}) detection for the cycloidal ring (with s=5 mm and $r_t=r_p$=5 mm) using the **AIm** algorithm.

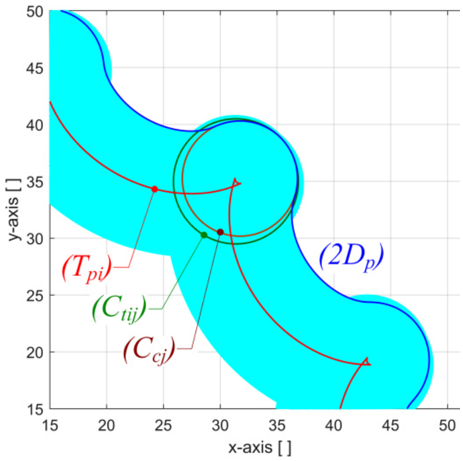

Fig. 18 – A zoomed-in detail on (T_{pi}) detection for the cycloidal ring (with s=5 mm and $r_t>r_p$ with r_t=5.5 mm) using the **AIm** algorithm.

Normally, the internal active surface of the cycloidal ring (being in gearing together the rotor through the rotary pins) is manufactured by several successive machining sequences of internal 2D contour milling. A milling allowance is left between two successive sequences (the active surface being intentionally undersized before the next sequence).

There is a simple way to detect the (T_{pi}) path in this approach (already presented in section 3). As example, in internal 2D contour milling the (T_{pi}) path with an allowance a before a final milling sequence is defined with a hypothetical milling tool having the radius r_t+a but the manufacturing is done with a real milling tool having the radius r_t. Figure 19 describes with a zoom-in detail (similarly with Fig. 5 and Fig. 7) this approach (with r_t=4 mm and a=0.5 mm). It is obvious that the internal envelope of the positions of circles (C_{cj}) is shifted inside with a distance a.

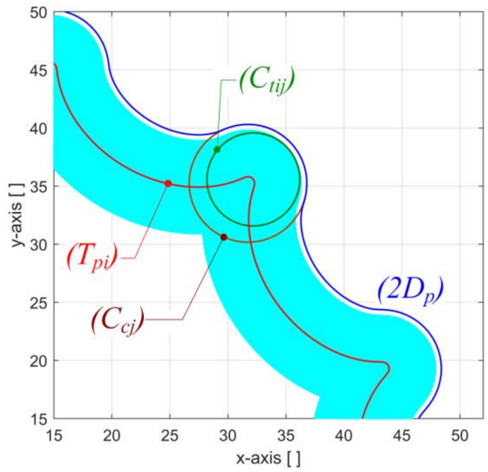

Fig. 19 – A zoomed-in detail on (T_{pi}) detection for a cycloidal ring manufacture (s=5 mm and milling allowance a=0.5 mm) using the **AIm** algorithm.

Frequently the final manufacturing process is the 2D contour grinding using a jig grinding wheel as tool (in internal or external grinding) having the radius r_t. The final (T_{pi}) or (T_{pe}) path for grinding is established in the same way (with an appropriate value of allowance a).

5. Conclusions and future work

A study on the tool path during manufacturing of some important parts inside the cycloidal reducers (having rotary pins as gear teeth placed on stator or rotor) was done in this paper. These paths are involved in manufacturing by 2D contours milling (using end mill cutters) for the external active surface on a cycloidal disc (in gearing with a cycloidal ring having the rotary pins as gear teeth) or for the internal active surface on a cycloidal ring (in gearing with a cycloidal disc having the rotary pins as gear teeth).

The tool axis trajectory is established related to a known 2D profiles of cycloidal disc or cycloidal ring, previously defined in a fixed Cartesian coordinate system (Horodinca *et al.*, 2022a, b) and a known radius of the tool. Two different algorithms for calculus of these tool paths were established for internal milling and two for external milling, one algorithm was finally chosen as being appropriate for each type of milling. Some simulations in Matlab were done in order to prove the availability of these chosen algorithms in definition of tool paths in some particularly conditions (milling tool radius, 2D profile shift, manufacturing allowance). The defined tool paths are available for manufacturing in 2D contour milling.

This study can be useful for manufacturing of active surfaces of other types of cylindrical internal gears (e.g. for sine gears, Horodinca, 2020).

However we should mention a first limitation of this study (solvable in a future approach): the distance between each two points on tool path is variable. This is clearly indicated by C_2 irregularities on Fig. 3 and Fig. 5 (for a particularly shape of a cycloidal disc).

There is a second limitation if this study is extent to manufacturing of some other 2D closed profiles by 2D contour milling. The steps **CS5a** or **CS6a** involved in internal milling **Im** (and **AIm** algorithm) or in external milling **Em** (and **AEm** algorithm) cannot produce a decision if $d_{1j} = d_{2j}$. Fortunately this situation never happens in cylindrical internal gears manufactured by 2D contour milling, particularly cycloidal disc or ring.

In the future the construction of a prototype of cycloidal reducer with the input motion at cycloidal ring and the output at rotor will be done by using some results of this approach.

REFERENCES

Allotta B., Fiorineschi L., Papini S., Pugi L., Rotini F., Rindi A., *Redesigning the Cycloidal Drive for Innovative Applications in Machines for Smart Construction Yards*, World Journal of Engineering, **18**, *2,* 302-315 (2021).

Dion J.L., Pawelski Z., Chianca V., Zdziennicki Z., Peyret N., Uszpolewicz G., Ormezowski J., Mitukiewicz G., Lelasseux X., *Theoretical and Experimental Study for an Improved Cycloid Drive Model*, Journal of Applied Mechanics, **87**, *1*, ffhal-03182247f (2020).

Han L., Gao X.S., Li H., *Space cutter radius compensation method for free form surface end milling*, The International Journal of Advanced Manufacturing Technology, **67**, *August 2013*, 2563-2575 (2013).

Horodinca M., *An approach on simulation of sine gear profile used on cylindrical gears*, Buletinul Institutului Politehnic din Iași, **66 (70)**, *2*, s. Machines Manufacturing, 37-52 (2020).

Horodinca M., Bumbu N.E., Munteanu A., Chitariu D.F., Chifan F., *A Study on the Synthesis of 2D Profiles for Cycloidal Discs Used in Cycloidal Reducers*, Buletinul Institutului Politehnic din Iași, **68 (72)**, *4*, s. Machines Manufacturing, 65-84 (2022).

Horodinca M., Bumbu E.N., Chitariu D.F., Munteanu A., Chifan F., Frigura G.I., *A Study of 2D Profile for a Cycloidal Ring Used in a Cycloidal Reducer*, Buletinul Institutului Politehnic din Iași, **68 (72)**, *4*, s. Machines Manufacturing, 85-99 (2022).

Lai Y., *The Working Principle and Parameter Design Method of Cycloidal Pinwheel Reducer*, Journal of Engineering Mechanics and Machinery, 7, *3,* 27-34 (2022).

Li T., An X., Deng X., Li J., Li Y., *A New Tooth Profile Modification Method of Cycloidal Gears in Precision Reducers for Robots*, Applied Sciences, **10**, *4* 1266 (2020), 10.

Lu L.S., Zhang F.X., Wan Z.P., Tang Y*., Cycloidal Gear Tooth Profile Modification of RV Reducer Based on Backlash Optimization*, Journal of South China University of Technology (Natural Science) **46**, *9*,1-8 (2018).

Petrovic N., Blagojevic M., Marjanovic N., Matejic M., *Parametric Drawing of a Cyclo Drive Shortened Equidistant Epitrochoid Gear*, Proc. of the 7th International Quality Conference, May 24th, 2013, Center for Quality, Faculty of Engineering, University of Kragujevac, Serbia, 303-308.

Shin J.H., Kwon S.M., *On the Lobe Profile Design in a Cycloid Reducer Using Instant Velocity Center*, Mechanism and Machine Theory, **41**, *5*, 596-616 (2006).

Yue Q.Q., Yu H., *Application of Cutter Radius Compensation in CNC Machining*, Applied Mechanics and Materials, **130-134**, 3585-3588 (2011).

Wang J., Luo S., Su D., *Multi-objective Optimal Design of Cycloid Speed Reducer Based on Genetic Algorithm*, Mechanism and Machine Theory, **102**, 135-148 (2016).

*** *Learning CNC Strategies and Tips*, https://cnc-programming-tips.blogspot.com/2014/12/g40-g41-and-g42-cuttercompensation.html (accessed at 21.01.2023).

*** *Circle Defined by 3 Points Calculator*, http://www.ambrnet.com/TrigoCalc/Circle3D.htm (accessed at 21.01.2023).

UN STUDIU PRIVIND DETERMINAREA TRAIECTORIEI SCULEI PENTRU REALIZAREA PRIN FREZARE DE CONTURARE 2D A DISCURILOR RESPECTIV A INELELOR CICLOIDALE UTILIZATE ÎN REDUCTOARELE CICLOIDALE

(Rezumat)

Lucrarea prezintă un studiu privind determinarea traiectoriei axei sculei utilizate în fabricarea prin frezare de conturare 2D (utilizând o freză cilindro-frontală) a unui disc cicloidal și a unui inel cicloidal utilizate în construcția unui reductor cicloidal în două variante diferite: cu bolțuri rotative plasate pe stator (ca dinți de dantură aflați în angrenare cu discul cicloidal) și cu bolțuri rotative plasate pe rotor (ca dinți de dantură aflați în angrenare cu inelul cicloidal). Aceste traiectorii trebuie descrise prin coordonatele punctelor parcurse de axa sculei într-un sistem cartezian. Pentru determinarea acestor traiectorii (având forma unei epicicloide sau a unei hipocicloide deformate) se utilizează profilele 2D ale discului respectiv ale inelului cicloidal într-o secțiune transversală precum și facilitățile oferite de geometria analitică. Chiar dacă determinarea acestor traiectorii este rezolvabilă pe mașinile de frezat CNC prin comenzi de compensare după valoarea razei sculei, unele particularități ale profilelor 2D ale discului respectiv ale inelului cicloidal impun o abordare specifică. Sunt propuse, verificate și validate prin simulare în Matlab o serie de algoritmi diferiți de determinare a traiectoriei sculei.